Journal of The Electrochemical Society

Going Beyond Sweep Voltammetry: Alternative Approaches in Search of the Elusive Electrochemical Stability of Polymer Electrolytes

Journal of The Electrochemical Society, 2021 **168** 100523

Going Beyond Sweep Voltammetry: Alternative Approaches in Search of the Elusive Electrochemical Stability of Polymer Electrolytes

Guiomar Hernández, Isabell L. Johansson,[=] Alma Mathew,[=] Christofer Sångeland,[=] Daniel Brandell, and Jonas Mindemark[z]

Department of Chemistry—Ångström Laboratory, Uppsala University, SE 751 21 Uppsala, Sweden

Solid polymer electrolytes (SPEs) are promising candidates for solid-state lithium-ion batteries. Potentially, they can be used with lithium metal anodes and high-voltage cathodes, provided that their electrochemical stability is sufficient. Thus far, the oxidative stability has largely been asserted based on results obtained with sweep voltammetry, which are often determined and reliant on arbitrary assessments that are highly dependent on the experimental conditions and do not take the interaction between the electrolyte and the electrode material into account. In this study, alternative techniques are introduced to address the pitfalls of sweep voltammetry for determining the oxidative stability of SPEs. Staircase voltammetry involves static conditions and eliminates the kinetic aspects of sweep voltammetry, and coupled with impedance spectroscopy provides information of changes in resistance and interphase layer formation. Synthetic charge–discharge profile voltammetry applies the real voltage profile of the active material of interest. The added effect of the electrode active material is investigated with a cut-off increase cell cycling method where the upper cut-off voltage during galvanostatic cycling is gradually increased. The feasibility of these techniques has been tested with both poly(ethylene oxide) and poly(trimethylene carbonate) combined with LiTFSI, thereby showing the applicability for several categories of SPEs.

 [DOI: 10.1149/1945-7111/ac2d8b]

Manuscript submitted August 27, 2021; revised manuscript received September 25, 2021. Published October 19, 2021.

Supplementary material for this article is available online

Next-generation high-energy-density batteries with lithium metal anodes and high-voltage cathode materials will require solid electrolytes that are more stable and safer than their liquid counterparts. In particular, solid polymer electrolytes (SPEs) constitute promising alternatives because of their wettability and adhesion to the electrodes, reduced flammability, scalability in production and being potentially low-cost.[1,2] Compatibility with lithium metal anodes and an inherent ability to resist dendrite growth are often cited as motivational factors and have been widely studied for SPE-based batteries.[3–6] Improved electrochemical stability compared to liquid electrolytes is also commonly cited as a motivation for solid-state electrolytes, but it is not clear whether this criterion is actually met. This ultimately comes down to a combination of clearly defining the electrochemical stability and finding suitable techniques to estimate this property correctly.

It could be argued that there exists quite some confusion in the literature regarding the electrochemical stability limits of electrolytes. A common misconception is, for example, the perceived equivalence between the anodic (oxidation) and cathodic (reduction) stability limits, and the HOMO and LUMO levels of the electrolyte.[7] While the HOMO and LUMO are molecular properties that may be obtained from the electronic structures of isolated molecules, redox potentials are thermodynamic properties that are dependent not only on the reacting molecules, but also their surroundings, concentration and the products formed in the reaction. This may lead to impossibly large electrochemical stability windows (ESWs) being suggested from, e.g., HOMO and LUMO levels obtained from density functional theory (DFT) calculations.[2,8] Moreover, the solvent and salt in conjunction must be taken into consideration as the electrolyte solution has its own distinct redox properties that are different from either of the individual components.[9]

The upper and lower potential limits of the ESW are typically determined from either linear sweep voltammetry (LSV) or cyclic voltammetry (CV). In both these techniques, the potential is ramped linearly versus time while the current is being measured. An increase in current is taken as an indication of degradation of the electrolyte at the working electrode interface, which is then expressed in the form of an electrochemical stability limit for the electrolyte. Being quick and easily applied techniques, LSV and CV have found widespread use for the determination of electrochemical stability limits. However, while the application of these techniques is relatively straightforward, the interpretation of the generated data is not.[10,11]

One key issue with voltammetry techniques is how to define when a current increase is sufficiently large to be considered the result of irreversible electrochemical degradation of the electrolyte. For reversible reactions, the thermodynamic redox potential can be unambiguously determined as the mid-point between the anodic and cathodic waves but for an irreversible reaction, this is simply not possible. Often, an inherently arbitrary current cut-off is used to define the onset of degradation, although this approach lacks theoretical significance.[12] The current response will also depend on the scan rate[13] and the thickness and conductivity of the electrolyte, as mass transport in the electrolyte governs the electrochemical response. Because of limited ionic conductivities and a propensity for poor electrode wetting, this will be especially problematic for solid electrolytes. Together, this further complicates the use of absolute current cut-offs. An alternative approach defines the electrochemical stability limit as the intercept of the (approximately) linear regions of the current–voltage curves before and after degradation.[13,14] Instead, this leads to the problem of where to draw the tangent of the exponential curve, which is often observed during electrolyte degradation.

As the voltage is continuously swept, the effects of reaction thermodynamics and kinetics become intertwined and difficult to differentiate. As a result, any catalytic effects of the working electrode surface will influence the results.[10,13] This questions the validity and relevance of stability limits obtained using "inert" electrodes such as stainless steel, aluminum, or glassy carbon, as they do not mimic the real surfaces found in Li-ion batteries. Other processes will occur in a realistic battery cell, which are not captured using inert electrodes.

Thus, even though voltammetry techniques provide some information about the SPE stability, the effect of the active material surface is ignored.[10,15] This becomes evident when reviewing the

[=]These authors contributed equally to this work.
[z]E-mail: jonas.mindemark@kemi.uu.se

bulk of SPE literature; although many papers report SPEs having high oxidation stability and claim that they can potentially be used with high-voltage cathodes, they are often only tested together with $LiFePO_4$, that has a rather moderate redox plateau at 3.5 V vs Li^+/Li, and not with high-voltage cathodes. Among the few examples that are cycled with high-voltage cathodes, rapid cell failure is commonly seen.[5,16,17] In the case of PEO-based SPEs a voltage plateau at 4.6 V vs Li^+/Li is observed upon overcharge of several active materials followed by a sudden drop in voltage, which has been assigned to the oxidation of the electrolyte.[5] However, other factors could affect this observed behavior besides the oxidative stability of the SPE, for example the mechanical stability and the compatibility with lithium metal and different active materials and surfaces.[17]

In order to overcome some of the limitations of the established voltammetry techniques, we have here developed different electrochemical techniques that can be used to investigate the electrochemical stability of SPEs. To demonstrate the feasibility of the techniques and how the results correlate for each technique, we have compared two model electrolytes based on poly(ethylene oxide) (PEO) and poly(trimethylene carbonate) (PTMC) with the same LiTFSI salt commonly used in SPEs. Several questions thereby arise. First, is there a single and appropriate technique or method to measure the ESW of SPEs? Second, does an SPE have a specific and well-defined ESW? Finally, how can the ESW be estimated for an electrochemically relevant system, i.e., a system that combines SPEs with the same electrodes as the desired application?

Experimental

Materials.—Poly(ethylene oxide) (PEO; Sigma-Aldrich, M_v: 2 000 000 g mol^{-1}), acetonitrile (ACN; Sigma Aldrich, 99.8%, anhydrous), lithium bis(trifluoromethanesulfonyl)imide salt (LiTFSI; BASF), lithium foil (Cyprus Foote Mineral Co, 125 μm), stainless steel foil (Sigma-Aldrich, AISI 316 alloy, 25 μm). All materials were used as-received and stored under inert conditions unless stated otherwise.

Preparation of polymer electrolyte films.—Poly(trimethylene carbonate) (PTMC) was prepared as previously described.[18] PTMC and PEO were dissolved in ACN along with 22 wt % LiTFSI and stirred at 40 °C overnight. The salt content was chosen as equivalent to 1 M concentration typically used in liquid electrolytes, which is also close to the optimal concentration reported for PEO and PTMC. The ratio of polymer to solvent was 0.04 and 0.03 g ml^{-1} for PTMC and PEO, respectively. Next, 2 ml of polymer electrolyte solution was cast in PTFE molds (20 mm in diameter). The solvent was removed by heating under vacuum for 60 h, see previous publication for experimental details.[19] Afterwards, the self-standing films could be cut to the desired diameter for testing.

Ionic conductivity.—The ionic conductivity of the SPEs was measured by electrochemical impedance spectroscopy using a Schlumberger SI 1260 Impedance/Gain Phase Analyzer, over the frequency range from 10 MHz to 1 Hz with an amplitude of 10 mV. The SPEs, with known diameter and thickness, were sandwiched between the stainless steel electrodes of the CR2025 coin cell, and annealed at 100 °C for 1 h the day before the measurement.

Cyclic voltammetry (CV).—Solid-state cells were assembled in CR2025-type coin cells by sandwiching the polymer electrolyte film (16 mm in diameter) between a lithium metal foil (15 mm in diameter) and a stainless steel foil (16 mm in diameter). Voltammetry measurements were carried out on either SP-240 or SP-300 potentiostats (Bio-Logic). Following the establishment of a stable open circuit voltage at 60 °C, measurements were recorded between 3 and 5 V vs Li^+/Li at different scan rates. For the scan rates 10 mV s^{-1} and 1 mV s^{-1}, five cycles were recorded.

Staircase voltammetry (SV).—Two electrode cells consisting of a lithium metal counter/reference electrode (15 mm in diameter), stainless steel working electrode (16 mm in diameter) and a PTMC: LiTFSI or PEO:LiTFSI polymer electrolyte membrane (17 mm in diameter) were hermetically sealed in coin cells (Hohsen, 2025). Cells were stored at 60 °C for 72 h prior to measurement. Using an SP-240 potentiostat (Bio-Logic), the chronoamperometric response was measured from 3–5 V vs Li^+/Li at steps of 100 mV, each held for 1 h, at 60 °C. Each step was followed by a 1 h pause, thereafter an electrochemical impedance spectroscopy (EIS) measurement and a second 10 min pause before the next potential step. EIS was done with an amplitude of 10 mV between 1 MHz and 100 mHz. Fitting of EIS data using equivalent circuits was done in ZView v. 3.2b.

Synthetic charge–discharge profile voltammetry (SCPV).—$LiFePO_4$ (LFP, Phostech Lithium), $LiNi_{1/3}Mn_{1/3}Co_{1/3}O_2$ (NMC, Customcells Itzehoe GmbH) and $LiNi_{0.5}Mn_{1.5}O_4$ (LNMO, Haldor Topsoe) electrodes were prepared by mixing 90 wt% active material, 5 wt% super C65 (Imerys) and 5 wt% carboxymethyl cellulose (Leclanché) in water with a MM 400 mixer mill (Retsch) for 30 min at 25 Hz. The obtained slurry was cast on carbon-coated Al foil and dried at room temperature for 24 h. LFP, NMC and LNMO half-cells were made with 13 mm diameter working electrode and 15 mm diameter metallic lithium (125 μm thick, Cyprus Foote Mineral) counter/ reference electrode in coin cells (CR2025, Ni-plated). 80 μl 1 M $LiPF_6$ in 1:1 w/w ethylene carbonate and diethyl carbonate (LP40, Gotion) electrolyte was used, soaked in two monolayer microporous polypropylene separators (Celgard 2500, 16 mm diameter). The voltage profiles were obtained by cycling the LFP, NMC, and LNMO half-cells at C/20 at room temperature in an Arbin BT cycler. The cycling voltage ranges for LFP, NMC, and LNMO cells were 2.7–4.2 V, 3.5–4.3 V, and 3.5–5 V vs Li^+/Li, respectively.

For the SCPV measurements, two electrode coin cells were made with stainless steel working electrode (16 mm in diameter), lithium metal as counter/ reference electrode (13 mm in diameter) and the polymer electrolyte (PEO:LiTFSI and PTMC:LiTFSI) (15 mm in diameter) in between the electrodes. Before the measurement, the cells were at open circuit voltage for 10 h at 60 °C. To conduct the SCPV experiments, the potential–time profile of the fifth charge of the half-cells with LFP, NMC and LNMO was interpolated to obtain the potential–time table with about 1000 data points evenly spaced in terms of potential. Using the "Potentio Profile Importation" (PPI) technique, this table was then imported into the instrument software (EC lab, version 10.12). All the SCPV measurements were performed using a VMP2 potentiostat (Bio-Logic) at 60 °C.

Cut-off increase cell cycling (CICC).—Three different positive electrodes made of LFP, NMC and LNMO were prepared as described in the previous SCPV section. The electrodes were cut in 22 mm diameter discs and the outer part of the electrode coating was removed, leaving an electrode coating diameter of 13 mm. The electrodes were further dried under vacuum at 120 °C overnight. The final mass loading of the electrodes was around 4 mg cm^{-2}. Polymer electrolyte solutions for casting PEO:LiTFSI were the same as aforementioned, but a higher concentration was prepared for PTMC: LiTFSI to increase the thickness of the SPE (the ratio of polymer to solvent was 0.05 g ml^{-1}). Polymer electrolyte casting was done as aforementioned but the solution was cast directly onto the cathodes. This procedure was done to ensure that the lithium metal and the polymer electrolyte covered the full electrode material surface and to avoid short circuits. The thickness of the SPE between cathode and anode was 100 and 120 μm for PEO:LiTFSI and PTMC:LiTFSI, respectively. Coin cells were assembled with a lithium metal disc of 14 mm diameter as counter/ reference electrode.

Cells were rested at 60 °C for 24 h before galvanostatic cycling was performed at C/20 at 60 °C. The upper cut-off voltage was

increased 0.1 V every 5 cycles until 5 V vs Li^+/Li while monitoring the voltage profile and capacity evolution. LFP was cycled between 2.7 and 3.7–5 V vs Li^+/Li, NMC between 3.5 and 4.2–5 V vs Li^+/Li, and LNMO between 3.5 and 4.6–5 V vs Li^+/Li. Current interruptions were made for 1 s at 5 min intervals following the analysis procedure reported by Lacey et al.[20,21]

Results and Discussion

The aim of this study is to determine whether it is possible to unambiguously and reliably determine electrochemical stability limits for SPEs. To answer this question and to illustrate the utilized techniques, we have measured the anodic stability of two model SPEs—PEO:LiTFSI and PTMC:LiTFSI, each with 22 wt% salt—in an attempt to also determine which of these electrolytes exhibits the highest oxidation stability. The electrolytes are distinguished by having different chemical structures (ether vs carbonate coordinating moieties), different coordination strengths and different ionic conductivities.[22] In the case of PTMC:LiTFSI, the ESW has previously been estimated to 5 V vs Li^+/Li,[18] whereas for PEO:LiTFSI many different values have been reported starting from 3.8 to 5.7 V vs Li^+/Li.[23–27] The broad range clearly demonstrates the arbitrariness of the employed techniques. The ionic conductivity of the electrolytes was determined to be 4×10^{-5} and 4×10^{-7} S cm^{-1} at 60 °C for PEO:LiTFSI and PTMC:LiTFSI, respectively, see Fig. S1 (available online at stacks.iop.org/JES/168/100523/mmedia).

In addition to LSV, CV is the technique most commonly employed to examine the electrochemical stability of SPEs. Different authors utilize different scan rates, making comparisons difficult due to its effect on reaction rates and the observed current magnitude. To illustrate the scan rate dependence, CVs were obtained at three different scan rates for PTMC:LiTFSI and PEO:LiTFSI; in Figs. 1a and 1b the first scan from OCV to 5 V is shown. Scan rates were chosen based on what is prevalent in the literature; 10 mV s^{-1} is among the highest scan rates typically employed, 1 mV s^{-1} is also common as an intermediate scan rate. 0.1 mV s^{-1} is seen in some papers and it brings the measurement closer to what the material would experience during galvanostatic cycling, as it takes approximately 5.5 h to go from OCV to 5 V, which is on the same time scale as battery cycling at C/5.

Due to the difference in ionic conductivity, the PEO:LiTFSI samples consistently display a higher current than the PTMC:LiTFSI electrolytes in these CV measurements (Fig. S2). This complicates the determination of the oxidative stability and the comparison between the two samples. Particularly, this observation shows the limitations of using the commonly employed current cut-off method. To more accurately spot the changes in the CVs, the derivative of the current may be used (Figs. 1e and 1f).[28] A small peak before the final increase in current can be seen in the derivative plots for both SPEs at all scan rates. The onset of those peaks appears at around 3.5 and 3.8 V vs Li^+/Li for PEO:LiTFSI and PTMC:LiTFSI, respectively. Again, determination of these values will largely depend on the *y*-axis scale. A more pronounced and continuous current increase is observed at higher potentials. The oxidative stability of PEO:LiTFSI and PTMC:LiTFSI was calculated by taking the tangent of the degradation curve and determining the intercept with the baseline prior to degradation, as described by Mousavi et al.[13] Another widely used method is to naïvely pick a tangent based on the region where the current increases exponentially, extrapolating the line to $I = 0$ and the potential at this point is then considered to be the oxidation onset. However, the capacitive baseline current is ignored with this method. Furthermore, the given oxidation onset will be lower for systems which do not have a clear exponential current response; a comparison between systems will not be possible if they vary in this regard. Most importantly, the positioning of the tangent is subjective and thus influences the perceived stability.

At high scan rates (10 mV s^{-1}) the final increase in current occurs at 4.4 and 4.7 V vs Li^+/Li for PTMC:LiTFSI and PEO:LiTFSI, respectively. At a slower scan rate of 1 mV s^{-1}, the degradation is shifted to 4.5 and 4.8 V vs Li^+/Li for PTMC:LiTFSI and PEO:LiTFSI, respectively. At even lower scan rates, i.e. 0.1 mV s^{-1} (see Figs. 1c and 1d), the oxidative stability of PTMC:LiTFSI is not very clear due to the lack of a distinct baseline and degradation curve. Nevertheless, using the strategy by Mousavi et al. as described above, the oxidative stability limit was determined to 4.3 and 4.8 V vs Li^+/Li for PTMC:LiTFSI and PEO:LiTFSI, respectively. As these results clearly illustrate, the validity of ESWs determined using these techniques is largely undermined by the arbitrary placement of tangents when there is no clear inflection point on the curve. As can be clearly seen in Figs. 1e and 1f there is also always a significant current response at potentials immediately below the defined stability limit that is, by definition, ignored by the tangent method. Nevertheless, following the first CV sweep, PEO:LiTFSI appears to be more stable, although the increase in current seems exponential at higher potentials. In contrast, the current increases in a more linear fashion for PTMC:LiTFSI.

In liquid systems, mass transport limitation is seldom an issue due to the comparatively high ionic conductivity, and can also be mitigated by using a rotating disc electrode. Meanwhile, it is very difficult to avoid mass transport issues in solid electrolyte systems when running voltammetry measurements. Therefore, it is also important to consider the reversibility of the reactions occurring in the CV; these can be examined by running multiple sweeps, see Fig. S3. In both systems, the anodic current decreases with each subsequent cycle, suggesting that a passivating layer is formed. A relatively larger cathodic current is seen for the PTMC:LiTFSI samples compared to PEO:LiTFSI samples, suggesting that the reactions occurring between 3 and 5 V vs Li^+/Li for PTMC:LiTFSI are partially reversible. All degradation products are expected to be formed irreversibly, which would suggest that PTMC:LiTFSI—while less electrochemically stable—instead forms a more robust passivation layer that leads to an improved kinetic stability compared to PEO:LiTFSI on subsequent scans.

Another approach to the classical CV experiment, that focuses specifically on the reversibility of the response, was introduced by Xu et al. and later developed and applied to SPEs by Li et al.,[12,29] involves sequentially increasing the potential limit from OCV to higher potentials with each cycle. The oxidation threshold is then identified based on the ratio between the anodic and cathodic capacities for each sweep as a measure of the reversibility of the system. Once the anodic capacity exceeds the cathodic capacity, irreversible reactions have occurred. With this technique, PEO:LiTFSI exhibited irreversible oxidation starting at 3.6 V vs Li^+/Li, accompanied by a decrease in average molecular weight, which suggests polymer chain scission at high potentials.[29] Here, the oxidation threshold was defined as the point at which the Faradaic capacity was 1% of the cathodic capacity, yet again an arbitrary criterion for the onset of oxidation. Furthermore, similar to regular CV, the potential is ramped linearly with time, which does not take into consideration the mass transport limitations (even at low scan rates) or the combined effects of thermodynamics and kinetics, i.e. the system never gets a chance to reach equilibrium, contributing to the difficulties of distinguishing a well-defined electrochemical stability.

Staircase voltammetry.—The issue of conflating of thermodynamics and kinetics in sweep voltammetry can be addressed by staircase voltammetry (SV), where the potential is held constant for a certain time before moving to the next potential. In contrast to LSV (and CV), mass transport limitations and capacitive currents are largely filtered out as the system is allowed to approach an equilibrium. In addition, holding the potential constant resembles the static potential conditions in a Li-ion battery, where the redox reactions occur at relatively constant potentials. In this work, the potential was stepped from OCV to 5 V vs Li^+/Li in 100 mV increments while the current response was monitored. Each step was held for 1 h. Based on the current response seen in Figs. 2a and 2b, PTMC:LiTFSI and PEO:LiTFSI begin oxidizing at approximately

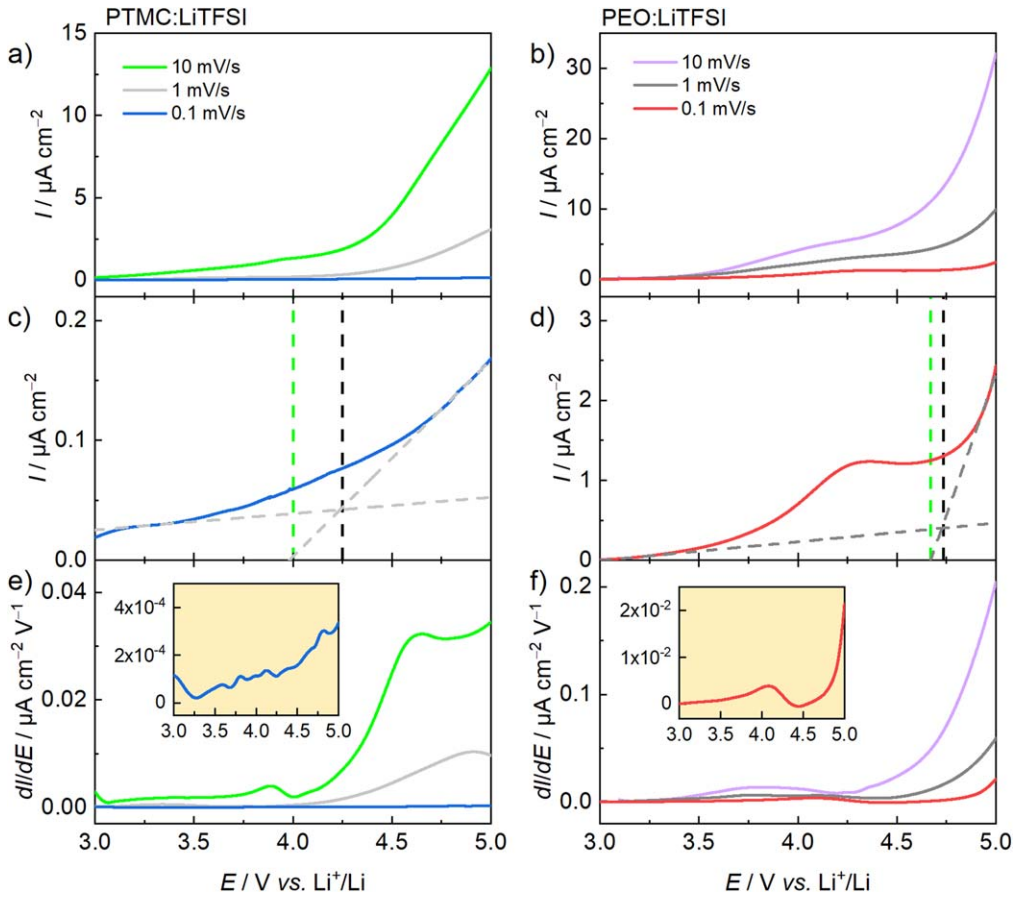

Figure 1. The current–voltage response of (a) PTMC:LiTFSI and (b) PEO:LiTFSI during the first forward scan at different scan rates at 60 °C. In (c) and (d) the dashed lines show the linear fits used to determine the oxidation onset at a scan rate of 0.1 mV s^{-1} for each SPE; the dashed green line represents the oxidation threshold based on the *x*-intercept of the degradation curve tangent and the dashed black line represents the oxidation threshold based on the intercept between the degradation current tangent and the baseline current tangent. The derivative with respect to potential for (e) PTMC:LiTFSI and (f) PEO:LiTFSI. The insets show the lowest scan rates at a higher magnification. Please note that the *y*-axis scale differs between PTMC:LiTFSI and PEO:LiTFSI.

3.8 and 3.5 V vs Li^+/Li, respectively. Above these potential thresholds, the current does not reach zero within 1 h, indicating a continuous oxidation reaction. This is in good agreement with the small peaks observed in the derivative of the current response in Figs. 1e and 1f. Interestingly, despite having very different ionic conductivities, the magnitude of the oxidation current is roughly equal in both systems, indicating that the ionic conductivity of PTMC:LiTFSI and PEO:LiTFSI is not a limiting factor when the potential is held for an extended time. This is in contrast to what was observed in the CVs in Figs. 1 and S2. However, the average relaxation current ($I_{relax.}$) at the end of each polarization step essentially mimics the LSV current response without the capacitive contribution, see Figs. 2c and 2d.

Between each potential step, electrochemical impedance spectroscopy (EIS) was measured in order to study changes in cell resistivity, see Fig. S4. The total interfacial resistance ($R_{int.}$) and polymer electrolyte resistance (R_{PTMC} or R_{PEO}) were extracted by fitting the impedance response using equivalent circuits, see Fig. S4. Based on the impedance response in Fig. 2 we note that the resistance of the bulk electrolyte in both PTMC:LiTFSI and PEO:LiTFSI steadily decreases during the measurement. Given the steady decline of R_{PTMC} and R_{PEO}, a likely explanation is that the SPE membranes gradually form better contact with the electrodes, resulting in a larger contact area and the appearance of a lower resistance, something commonly seen for PTMC electrolytes.[18,30] In the case of PEO, polymer chain scission at elevated potentials, and subsequent formation of lower-molecular-weight chains, could facilitate electrode wetting further.[29] Interestingly, coinciding with the decrease in $R_{int.}$, the current profile becomes erratic during each potential step in PEO:LiTFSI, see Fig. 2b. In the case of PTMC:LiTFSI, the reduction in R_{PTMC} is large enough to suppress an increase in $R_{int.}$ and as a result $R_{tot.}$ remains fairly constant. It should be noted, that this was observed despite keeping the cells at the measurement temperature (60 °C) for 72 h prior to measurement and the large molecular weights of PTMC and PEO: ∼360 000 and 2 000 000 g mol^{-1}, respectively. In addition, stack pressure exerted by the coin cell spring could potentially compress the polymer films, resulting in a lower resistance. However, given the large molecular weights of PTMC and PEO used herein, this would require very high compression forces to cause a significant reduction in thickness of the thin electrolyte films.

As seen in Figs. 2c and 2d, R_{int} in PTMC:LiTFSI and PEO:LiTFSI show similar behavior. Initially, R_{int} increases gradually from 1 to 1.8 kΩ between 3 and 4.1 V vs Li^+/Li in PTMC:LiTFSI. Likewise, an increase from 117 to 147 Ω can be observed in PEO:LiTFSI going from 3 to 4.5 V. Notably, R_{int} is much larger in PTMC:LiTFSI compared to PEO:LiTFSI. In both systems, R_{int} eventually peaks and then drops. In PTMC:LiTFSI, R_{int} drops from 1.8 to 1.4 kΩ between 4.2 to 4.6 V. CO_2 gas formation has been observed at 4.25 V vs Li^+/Li in PTMC:LiTFSI,[31] which coincides with the decrease in R_{int} observed here. In addition, SO_2 gas formation derived from salt decomposition has been observed at 4.4 V vs Li^+/Li.[31] Salt-derived species could initiate secondary reactions which affect the interfacial resistance. In PEO:LiTFSI, R_{int} decreases from 147 Ω to 106 Ω between 4.5 and 4.9 V, followed by a sharp increase. In contrast, PTMC:LiTFSI exhibits a slower increase in R_{int} from 4.8 V and onwards, suggesting that the failure mechanism is more abrupt in PEO:LiTFSI. However, it should be

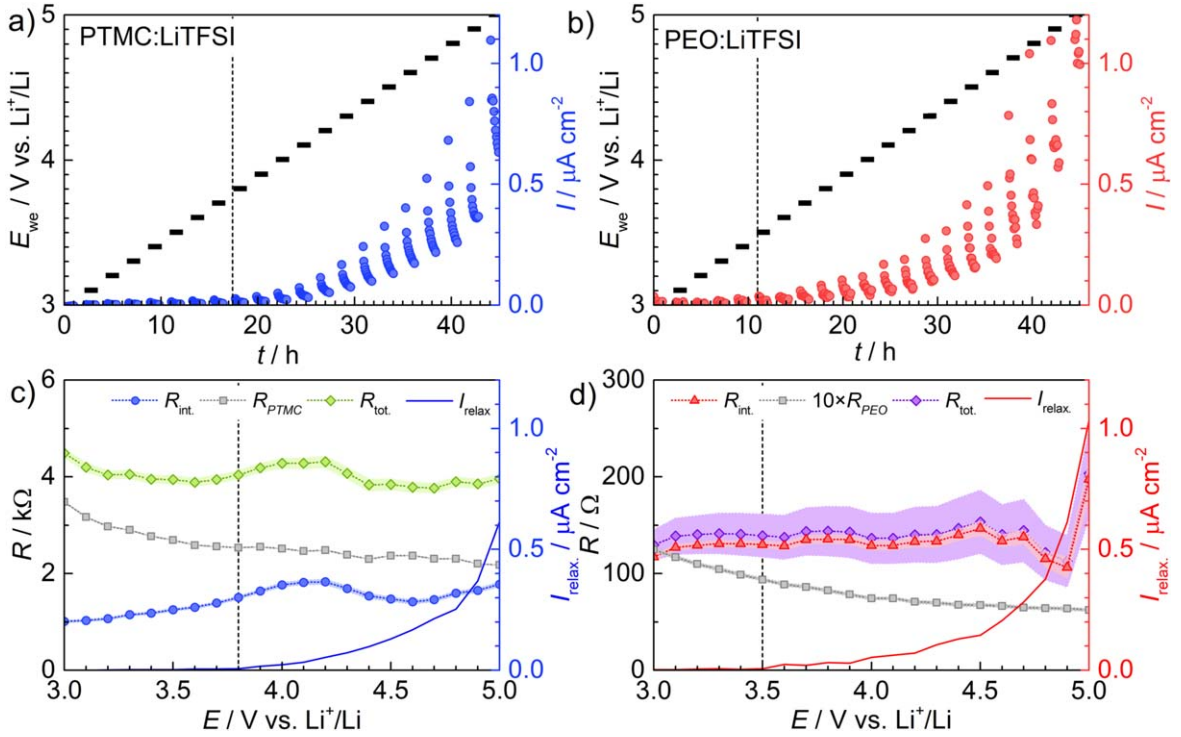

Figure 2. The current response of (a) PTMC:LiTFSI and (b) PEO:LiTFSI at different potential steps ranging from 3–5 V vs Li^+/Li. The relaxation current ($I_{relax.}$), bulk polymer resistance (R_{PTMC} or R_{PEO}), interfacial resistance ($R_{int.}$) and total resistance ($R_{tot.}$) for (c) PTMC:LiTFSI and (d) PEO:LiTFSI at different potentials. R_{PEO} has been multiplied by 10 to improve legibility. Absolute errors for $R_{int.}$, R_{PTMC}, R_{PEO} and $R_{tot.}$ are represented by the shaded area.

emphasized that the interfacial resistance is dominant in PEO:LiTFSI in contrast to PTMC:LiTFSI, where R_{int} and R_{PTMC} are of the same order of magnitude. Hence, any changes in R_{int} become more pronounced in the current response of PEO:LiTFSI.

Clearly, SV evaluates the stability of SPEs under more realistic voltage conditions, simplifies the data interpretation and allows for combination with EIS to gather more detailed information about the state of the electrochemical cell. In another incarnation, known as the *electrochemical floating test*, it can also be made to take into account the effects of the electrode active materials by utilizing an electroactive cathode material as the working electrode as opposed to an inert electrode and detecting the leakage current following a potential step.[32,33] Using this technique, a poly(dioxolane)-based SPE (with ether groups) exhibited a leakage current at 4.7 V vs Li^+/Li when tested against a $LiNi_{0.6}Mn_{0.2}Co_{0.2}O_2$ electrode.[33]

Synthetic charge–discharge profile voltammetry.—Considering the inherent issues of objectively assigning a threshold potential corresponding to the true thermodynamic stability limit, it can be questioned whether it is at all reasonable to attempt to determine an onset potential of degradation. With the influence of kinetic effects, perhaps the time domain (kinetics) is a more relevant parameter than potential? While the sweep and step voltammetry approaches typically utilize either a constant voltage scan rate or a constant length of the voltage steps, in a "real" battery system the instantaneous sweep rate will depend on the exact potential profile of the active material. Hence, the time spent in a particular potential range varies wildly between different materials. This is addressed in the synthetic charge–discharge profile voltammetry (SCPV) technique, which applies the potential profile of an active material of interest to an "inert" working electrode. As the potential is ramped exactly the same as it would be in a real-life battery containing the active material, SCPV provides for a more practical and realistic way of understanding and evaluating the anodic stability of the system.[34] Here, the anodic stability of the PEO:LiTFSI and PTMC:LiTFSI polymer electrolytes was assessed using the characteristic voltage profiles of $LiFePO_4$ (LFP), $LiNi_{1/3}Mn_{1/3}Co_{1/3}O_2$ (NMC) and $LiNi_{0.5}Mn_{1.5}O_4$ (LNMO) with the SCPV technique (Figs. 3a–3c). As observed in Fig. 3a, LFP has a long voltage plateau at ~3.45 V vs Li^+/Li corresponding to the Fe^{2+}/Fe^{3+} redox couple. The system

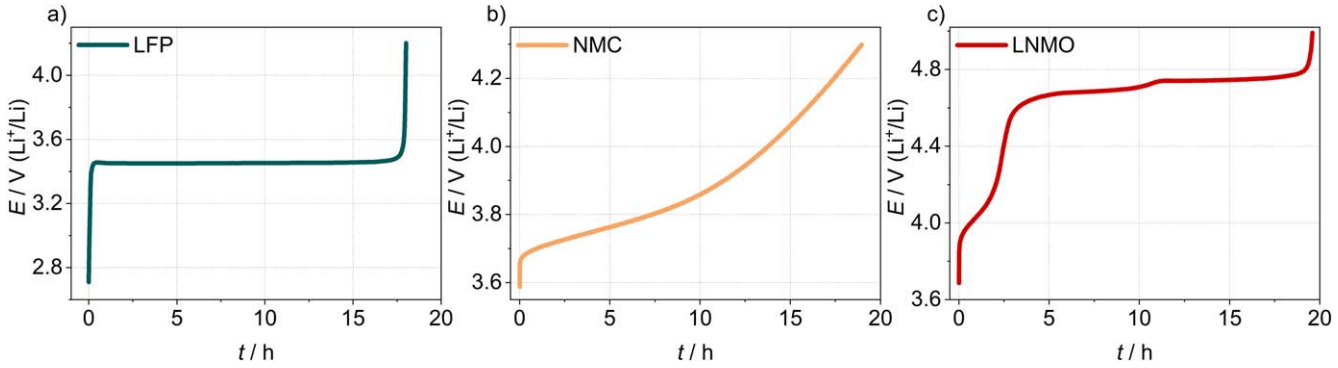

Figure 3. Delithiation profile of the 5th cycle of (a) LFP, (b) NMC, and (c) LNMO half-cells at C/20 with liquid electrolyte (LP40) at room temperature.

spends the majority of the time within this plateau during galvanostatic cycling and consequently also in the SCPV measurements. Unlike the LFP voltage profile, the NMC profile does not have a distinct voltage plateau (Fig. 3b). This indicates that the time spent in any voltage region is not necessarily longer than other regions, but it is also worth noting that the slope is not the same in every voltage region. LNMO is comparatively a higher-voltage cathode than LFP or NMC. The LNMO voltage profile shown in Fig. 3c has a minor plateau at ∼4.1 V vs Li^+/Li which is a feature of disordered-type LNMO, corresponding to the Mn^{3+}/Mn^{4+} redox couple. At ∼4.67 V and ∼4.74 V vs Li^+/Li, two voltage plateaus are observed, corresponding to the Ni^{2+}/Ni^{3+} and Ni^{3+}/Ni^{4+} redox couples. With lengthier voltage plateaus in LNMO, a greater amount of time is spent at these voltages than at other voltages.

The SCPV method measures the current passed with time which can also be represented against voltage (Figs. S5–S7). Another way to represent the data is with the amount of charge passed as shown in Fig. 4 for the LFP, NMC, and LNMO voltage profiles. For the LFP profile, we observe a constant increase in charge throughout the plateau region (i.e., ∼3.45 V vs Li^+/Li) in both PEO:LiTFSI and PTMC:LiTFSI, although the cell with PEO:LiTFSI passed more charge compared to the PTMC:LiTFSI cell. After the plateau region, the charge rises vertically in smaller amounts in both systems, but this occurs in a relatively short period of time when the potential rises from 3.45 V to 4.2 V vs Li^+/Li. Figures 4b and 4c show the amount of charge passed vs potential (Q vs E) and the corresponding differential capacity (dQ/dE vs E), respectively. The differential capacity plot aids the interpretation of the Q vs E plot as the peaks ideally only correspond to faradaic reactions since purely capacitive processes are constant in dQ/dE curves. The passing of charge is not a continuous process in the cycled voltage range, as shown in Fig. 4b, but is highly dependent on the amount of time spent at each potential, and the large peak in Fig. 4c corresponds to the large amount of time spent in a relatively narrow potential range in the plateau region. Notably, despite this plateau being in a supposedly stable potential region, as suggested by the CV and SV measurements, evidence of faradaic (decomposition) reactions is observed for both the PEO:LiTFSI and the PTMC:LiTFSI system, although the amount of charge is below 1 μAh cm^{-2}—negligible compared to the capacity of a battery with active material. The charge passed during the SCPV sweep is higher for PEO:LiTFSI (0.33 μAh cm^{-2}) than for PTMC:LiTFSI (0.085 μAh cm^{-2}). This higher observed extent of degradation reactions is consistent with the faster dynamics (both polymer chain and ionic) of the PEO:LiTFSI system in the context of time-dependent electrochemical stability. From the dQ/dE plot in Fig. 4c, it is also observed that the peak corresponding to the faradaic reaction in the case of PEO:LiTFSI is also broader compared to PTMC:LiTFSI, indicating a higher extent of oxidation in PEO:LiTFSI system in the vicinity of the plateau region. Beyond the plateau, starting at 3.8 V, the amount of charge rises faster for PTMC:LiTFSI compared to PEO:LiTFSI until the upper cut-off voltage is reached. This rise occurs in a region where the potential is swept much more rapidly and indicates the onset of more extensive decomposition, where the stability of PTMC:LiTFSI appears inferior

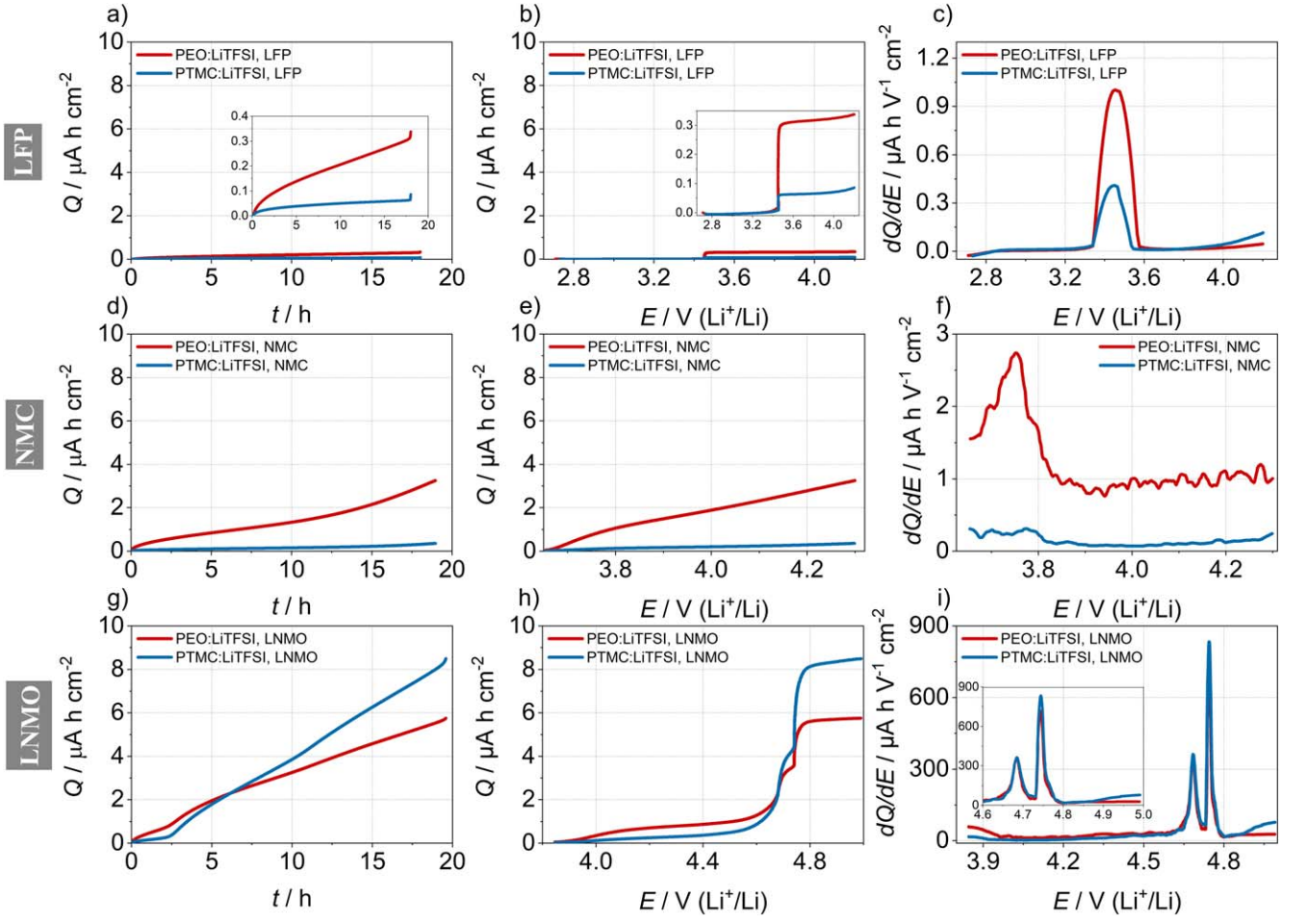

Figure 4. (a), (b) and (c) illustrate the amount of charge passed vs time (Q vs t), the amount of charge passed vs voltage (Q vs E) and the corresponding dQ/dE vs E plot, respectively, using the LFP voltage profile in the SCPV technique. The insets in (a) and (b) show the magnification of Q in the range 0–0.4 μAh cm^{-2}. (d), (e) and (f) show the same for the NMC voltage profile and (g), (h) and (i) show the SCPV data for the LNMO voltage profile. The inset in (i) shows the magnification in the range 4.6–5.0 V vs Li^+/Li.

to PEO:LiTFSI. This onset is in agreement with the SV technique where the oxidation of PTMC:LiTFSI was detected at 3.8 V vs Li^+/Li.

For the NMC-based profile (Fig. 3b), more charge was passed with PEO:LiTFSI (3.26 μAh cm^{-2}) than PTMC:LiTFSI (0.36 μAh cm^{-2}) in the SCPV anodic sweep (Fig. 4d). The amount of charge passed in PEO:LiTFSI is one order of magnitude higher using the NMC voltage profile than with LFP. The slope differences in both curves in Fig. 4d suggest that the charge passed does not have a direct relationship with time, but is instead dependent on the time spent at each voltage. Fig. 4f illustrates this correlation even more clearly, showing a clear peak for both electrolytes in the range of ~3.65–3.82 V vs Li^+/Li where more amount of charge is passed compared to other voltage regions where the charge derivative is more or less constant with increasing voltage. Again, degradation in this region is expected based on the SV results and the onset of degradation at the higher potentials with the LFP voltage profile. Overall, PEO:LiTFSI is observed to have a faster rate of oxidation than PTMC:LiTFSI.

The oxidative stability of the PEO:LiTFSI and PTMC:LiTFSI electrolytes was also evaluated using an LNMO voltage profile. Here, a longer time is spent at the higher plateaus (i.e., ~4.67 V and ~4.74 V vs Li^+/Li) than at other voltages. Figure 4h also illustrates a two-step rise in the amount of charge in the 4.6–4.8 V vs Li^+/Li range in both systems, corresponding to the two upper voltage plateaus characteristic of LNMO. PTMC:LiTFSI is seen to pass a relatively lower amount of charge until ~4.67 V vs Li^+/Li after which the system starts to experience a higher rate of degradation than the PEO:LiTFSI system, especially at the 4.74 V vs Li^+/Li plateau. After the plateau region, from 4.8 to 5 V, the charge seems to increase continuously for PTMC:LiTFSI which indicates further degradation of the electrolyte. At the end of the SCPV sweep, PTMC:LiTFSI passed ~8.48 μAh cm^{-2} of charge whereas PEO:LiTFSI passed ~5.75 μAh cm^{-2} of charge. In Fig. 4i, it is also possible to observe a remnant of the degradation reaction beginning from 3.84 V as observed in the *dQ/dE* plot using the NMC profile (Fig. 4f).

Overall, these results show a higher rate of degradation for PEO:LiTFSI at lower voltages following the LFP and NMC profiles compared to PTMC:LiTFSI. However, once higher voltages are reached, such as those with the LNMO profile, the degradation of PTMC:LiTFSI becomes more severe and occurs at a higher rate compared to PEO:LiTFSI. This suggests that PTMC:LiTFSI is more stable than PEO:LiTFSI under the conditions of operation of the LFP and NMC voltage profiles while the opposite is true at the higher potentials of the LNMO voltage profile. Importantly, we observe differences in the electrochemical response that are dependent not only on the applied voltage, but also how quickly the voltage is swept in different regions of the potential profile and the time spent in a particular potential region.

Cut-off increase cell cycling.—From the SCPV method, it is clear that time-dependent faradaic reactions can be observed even at relatively low potentials, where other methods indicate electrochemical stability. This adds further layers of complexity to determining the limits to the electrochemical stability of electrolytes. However, while the SCPV method mimics the potential profile of relevant electrochemical systems, it operates with an inert working electrode and therefore does not take into account the influence of the active material. Since the electrolyte stability is also influenced by the active material, its surface chemistry as well as the operating voltage of a battery,[5,10,12,15,35] it becomes less relevant to discuss or attempt to determine the electrochemical stability of an electrolyte in the absence of a relevant working electrode. Essentially, this means utilizing battery half-cells as relevant electrochemical systems to investigate the oxidative stability of the electrolyte under more realistic conditions to assess the practical electrochemical stability of the system. Our take at this is to propose a cut-off increase cell cycling (CICC) method, where the capacity and voltage are monitored during galvanostatic cycling while gradually increasing the upper cut-off voltages. The resulting voltage profiles give information about side reactions during cycling and at what voltage they occur. The irreversibility of such reactions can be monitored by the decrease in coulombic efficiency (CE) as irreversible degradation reactions result in excess charge capacities compared to discharge capacities. In addition, this method also shows the voltage at which cell failure occurs—all within an electrochemically relevant system. By using lithium metal as counter electrode, there is an infinite source of lithium that ensures that any lithium lost due to side reactions can easily be replenished and the lithium inventory is not a limiting factor in this method. To investigate the oxidative stability of PEO:LiTFSI and PTMC:LiTFSI in a broad voltage range, we have selected LFP, NMC and LNMO as cathode materials since they have distinct voltage profiles in different redox potential regions.

The different ionic conductivities of these SPEs at 60 °C lead to different resistances, as seen in Figs. 2 and S1, and different overpotentials that will affect the accessibility of the full capacity of the cell. Nevertheless, it should not have a large impact on the voltage at which side reactions or electrolyte degradation occurs. The voltage profile of LFP electrodes with each electrolyte is shown in Fig. 5. For LFP cathodes, with a characteristic plateau in the voltage profile, the discharge capacity does not change much when increasing the cut-off voltage, see Fig. 6a. However, a decrease in CE (Fig. 6b) indicates the appearance of side reactions. As such, it

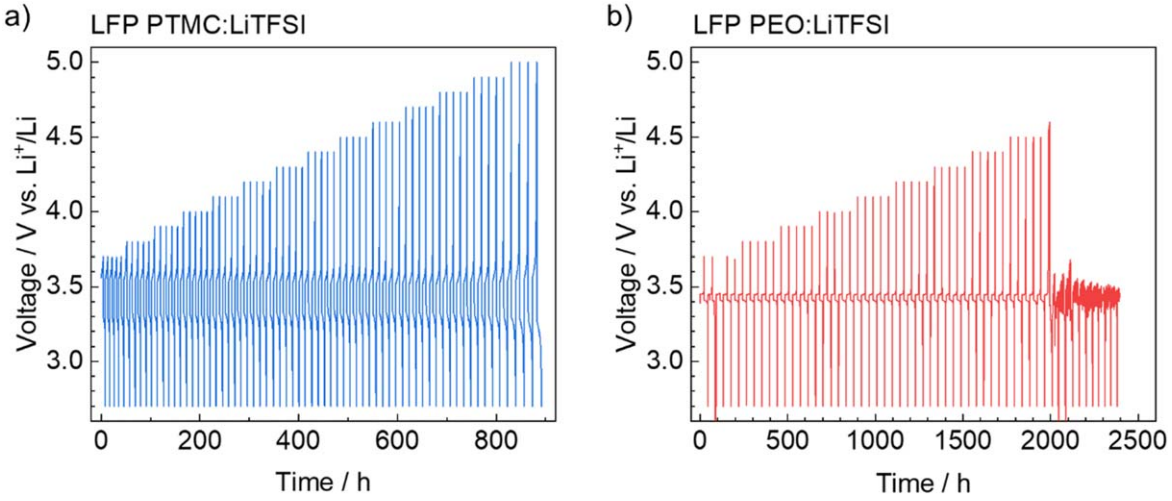

Figure 5. Voltage vs time profiles with the CICC method, where the upper cut-off voltage is increased every 5 cycles, for LFP half-cells with (a) PTMC:LiTFSI and (b) PEO:LiTFSI.

comprises a direct assessment of the reversibility of the working electrode reaction, similar to the reversible CV method reported by Li et al. for determining the ratio between the Faradaic and non-Faradaic reactions.[29]

The cell with PTMC:LiTFSI shows a decrease in CE when the voltage cut-off is 3.8 V vs Li^+/Li (i.e., at cycle 6) (Fig. 6b). These side reactions of PTMC:LiTFSI can also be seen as an additional plateau in the voltage profile above the redox plateau of LFP in the first cycle of each cut-off voltage (the cycles displayed in Fig. 6c), but this feature disappears in the cycles in between (Fig. S8a), suggesting that a passivating layer is formed on the electrodes. This also explains why the CE is lower for the first cycle and increases in the following four cycles within the same cut-off voltage. Due to insufficient initial electrode wetting, the full theoretical capacity is not achieved with PTMC:LiTFSI within the time frame of the experiment.[18,30] Instead, a low but gradually increasing discharge capacity is observed throughout the experiment, notably accelerating at 4.9 V vs Li^+/Li (cycle 60) (Fig. 6a). In the case of PEO:LiTFSI, side reactions are first identified at 4.3 V vs Li^+/Li (at cycle 31) (Fig. S8b), and they do not seem to be passivating the electrode as they are more pronounced with increasing cycle number and, consequently, there is a decrease in discharge capacity and CE (Figs. 6a and 6b). In addition, the cell with PEO:LiTFSI featured a sudden failure at 4.6 V vs Li^+/Li (cycle 46) (Fig. 6). The cell first shows an additional plateau at 4.55 V vs Li^+/Li in cycle 46 and afterwards an "infinite" charge at 3.5 V vs Li^+/Li that continued until the established time limit (30 h) was reached (Fig. 6d).

These results suggest that there are two ways to assess the stability of the system. First, the voltage at the onset of degradation when side reactions occur and the CE decreases. Second, a "catastrophic degradation" when a complete failure of the cell occurs. The latter can be detected as an "infinite" charging step or by a rapid voltage drop. Besides the oxidative stability of the system, these failure mechanisms could also be due to dendrite growth and penetration through the electrolyte, which would be more severe for the soft PEO:LiTFSI compared to the tougher PTMC:LiTFSI. However, the method employed here does allow the separation of both mechanisms. Nevertheless, considering the onset of degradation, the LFP cell with PEO:LiTFSI is more stable than PTMC:LiTFSI. However, if considering the catastrophic degradation, the cell with PTMC:LiTFSI would be more stable than PEO:LiTFSI, as the latter failed at 4.6 V vs Li^+/Li while the former does not fail during the experiment. The results indicate that each SPE has a different degradation mechanism. While PTMC:LiTFSI seems to degrade slightly but gradually as the voltage increases but with no clear cell failure, PEO:LiTFSI is more stable up to higher voltages but suffers from abrupt failure with a continuous charge step which indicates a continuous degradation of the electrolyte. These differences are in agreement with the voltammetry results that showed a more exponential degradation curve for PEO:LiTFSI compared to

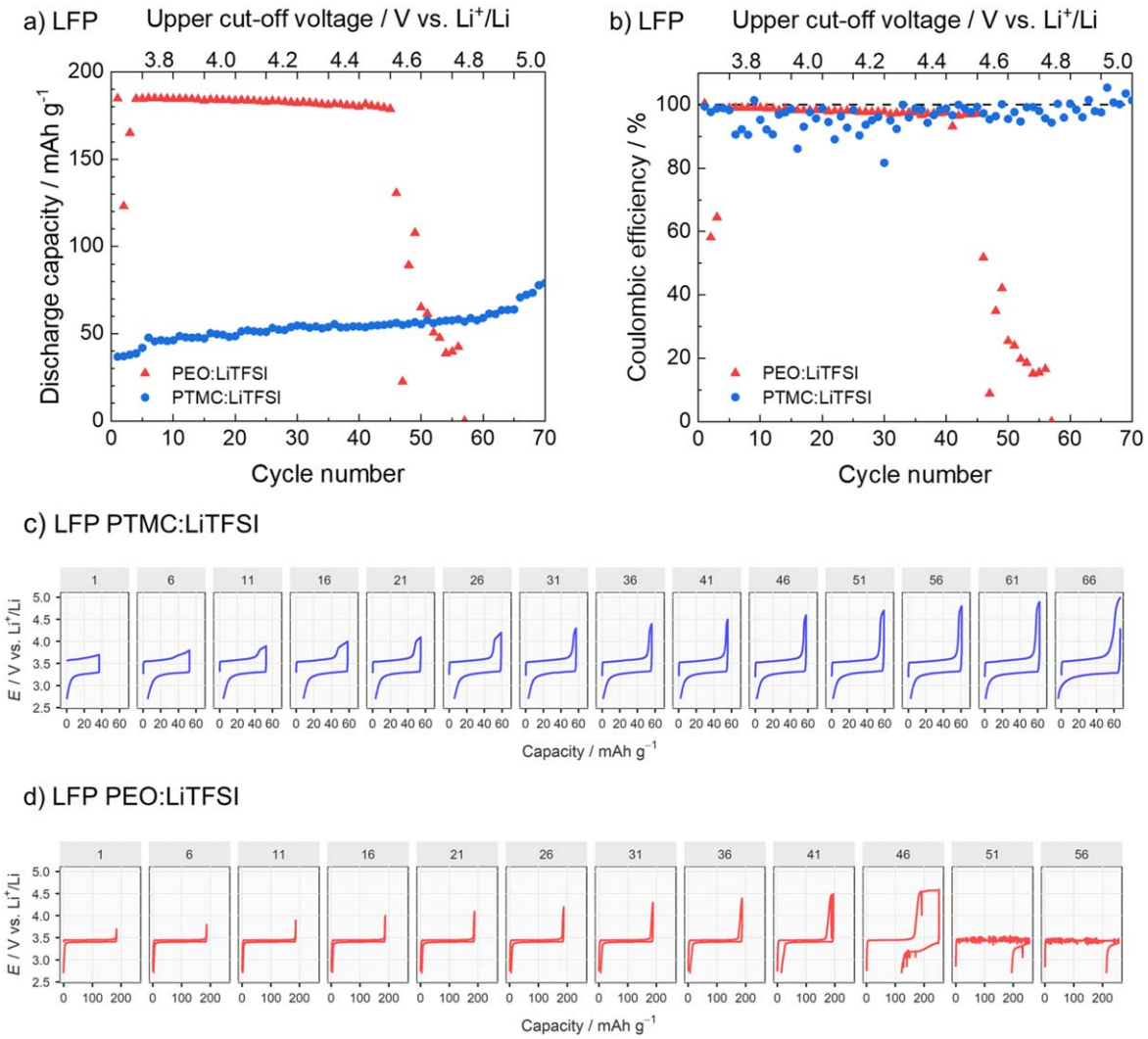

Figure 6. Results from the CICC method for LFP half-cells: (a) discharge capacity, (b) coulombic efficiency, (c) and (d) voltage profiles with PTMC:LiTFSI and PEO:LiTFSI, respectively, at different cycles with each cut-off voltage. The first upper cut-off voltage is 3.7 V vs Li^+/Li and it is increased with 0.1 V every 5 cycles until 5 V vs Li^+/Li or battery failure.

PTMC:LiTFSI, and could be the result of better passivation in PTMC:LiTFSI than in PEO:LiTFSI.

Analyzing the development of the internal resistance in the cell during the experiments contributes to a better understanding of the electrochemical degradation phenomena. While this can be done with EIS, the intermittent current interruption (ICI) technique allows for determination of the cell resistance simultaneously during cycling.[20,21] Figure 7 compares the interfacial and bulk resistances obtained using EIS with SV (in grey) and the average cell resistance from the last discharge at each voltage cut-off determined using ICI. As seen in Fig. 7a, the increase in $R_{int.}$ for PTMC:LiTFSI at around 3.8 V vs Li^+/Li could be explained by the side reactions observed during cycling. According to ICI, the cell resistance decreases until 4.6 V vs Li^+/Li which could be due to an improved electrolyte–electrode contact. PTMC-based electrolytes are well-known for gradually infiltrating the porous cathode, resulting in continuously increasing cell capacities as more of the capacity is accessed.[18,30] Although R_{bulk} continues to decrease all the way to 5 V vs Li^+/Li, both $R_{int.}$ and $R_{LFP\ cell}$ increase after 4.6 V, suggesting upcoming cell failure. In the case of PEO:LiTFSI, ICI analysis revealed that $R_{LFP\ cell}$ increased at a lower potential in comparison to R_{int}, see Fig. 7b. This discrepancy could reflect the effect of the LFP surface in contrast to the 'inert' stainless steel surface. Nevertheless, $R_{LFP\ cell}$ still exhibits the same behavior as seen before: initially, the resistance increases gradually. At a certain point, the resistance peaks, after which it decreases slightly. Shortly after, the resistance increased rapidly, also suggesting the upcoming cell failure. The final increase in resistance for both cells is much more pronounced for PEO:LiTFSI (increasing almost 4 times from 4.5 to 4.6 V vs Li^+/Li) than for PTMC:LiTFSI (doubles from 4.6 to 5 V vs Li^+/Li), which could explain the sudden failure observed with PEO:LiTFSI. This can also be correlated to the different oxidation behavior seen in the CV experiments for each SPE, as the PEO:LiTFSI shows a more exponential degradation curve.

In contrast to LFP, the voltage profile characteristic of NMC is not constant at a specific voltage, but is instead sloping. Therefore, it will affect the specific capacity obtained at each cut-off voltage. However, for the assessment of the electrochemical stability, the obtained capacity is less relevant than the reversibility of the system, i.e., the CE, which is not capacity-dependent. In general, the performance of NMC cells with both SPE systems is poorer compared to LFP cells. Although one reason could be the different redox potential of the active materials, the interfaces, cell resistance and catalytic reactions will also play an important role. As can be seen in Fig. 8a, the discharge capacity is low in the first cycle but increases in the following cycles and with increasing cut-off voltage until 4.4 V vs Li^+/Li (cycle 11) for the cell with PEO:LiTFSI and 4.7 V vs Li^+/Li (cycle 26) for PTMC:LiTFSI, which is an indication of a higher extent of delithiation of the active material with increasing cut-off voltage. The cell resistance of NMC with PEO:LiTFSI is lower than with PTMC:LiTFSI (Fig. S9), similar to what was observed with LFP electrodes. However, while it is of the same order of magnitude for LFP and NMC with PEO:LiTFSI, with PTMC:LiTFSI the resistance is doubled from LFP to NMC, which could explain the poorer cell performance with the latter active material.

In the case of PEO:LiTFSI, the capacity decreases when the number of cycles increases within the same cut-off voltage, suggesting the appearance of side reactions already at 4.3 V vs Li^+/Li, i.e. at cycle 6. This is also in agreement with the slight decrease in CE at the same voltage. However, a more drastic decrease in CE and discharge capacity is observed at 4.5 V vs Li^+/Li, and the cell failed at 4.7 V vs Li^+/Li at cycle 26 (Figs. 8 and S10). The cell failure characteristics of NMC with PEO:LiTFSI are as follows: the discharge capacity decreases at 4.5 V vs Li^+/Li; afterwards an additional redox plateau appears at around 4.65 V vs Li^+/Li followed by an "infinite" charge at 4 V vs Li^+/Li. Despite the initial decrease in capacity, these cell failure characteristics are similar to the what is observed with LFP although at slightly different voltages, which could indicate that it is characteristic of PEO:LiTFSI rather than the active material. In the case of NMC with PTMC:LiTFSI, the CE displays scattered values, but a trend can be spotted within the same cut-off voltage, starting at a low value and increasing afterwards. The highest CE is seen at 4.5 V vs Li^+/Li (cycle 20) and decreases thereafter (Fig. 8b). In contrast to the failure characteristics of the cell with PEO:LiTFSI, with PTMC:LiTFSI the overpotential increases throughout the cycling experiment and the capacity fades until 5 V vs Li^+/Li (Figs. 8a and S10). These results indicate that the degradation reactions in PTMC:LiTFSI yet again occur gradually while they are more abrupt with PEO:LiTFSI, and could yet again be indicative of more effective passivation in the PTMC:LiTFSI system.

Another common active material that would impose more challenges for the electrochemical stability of the electrolyte is LNMO, due to its high voltage plateau at around 4.7 V vs Li^+/Li. It thus constitutes a good example for investigating the electrochemical stability of a polymer electrolyte. With the PEO:LiTFSI electrolyte, the LNMO cells start failing at 4.7 V vs Li^+/Li (cycle 6), with the discharge capacity and CE decreasing rapidly within that cut-off voltage regime (Fig. 9). Complete failure occurred when the cut-off was increased to 4.8 V vs Li^+/Li (Fig. S11). In the case of PTMC:LiTFSI, on the other hand, the discharge capacity and coulombic efficiency are rather constant until 4.9 V vs Li^+/Li, i.e., cycle 16 (Fig. 9) corresponding to the lower redox plateau of manganese. Afterwards, the discharge capacity slightly increases due to the upper redox plateau of nickel until the cell fails when trying to reach 5 V vs Li^+/Li (Figs. S11 and 9). Another general observation from these results is that the initial plateau at around 4.0 V vs Li^+/Li corresponding to the manganese redox reaction disappears after the cut-off voltage is increased to 4.7 and to 4.9 V vs Li^+/Li for PEO:LiTFSI and PTMC:LiTFSI, respectively, as can be seen in Fig. S11. Regardless of the voltage at which the cell fails for each SPE, in both

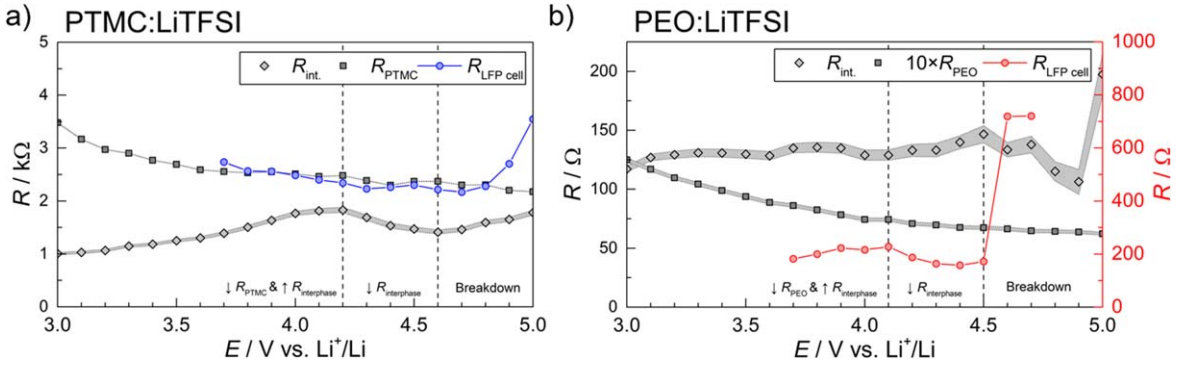

Figure 7. The bulk polymer resistance (R_{bulk}) and interfacial resistance ($R_{int.}$) from EIS, and the internal cell resistance from ICI ($R_{LFP\ cell}$) for a) PTMC:LiTFSI and b) PEO:LiTFSI at different potential steps. R_{PEO} has been multiplied by 10 to improve legibility. The absolute error for $R_{int.}$, R_{PTMC}, R_{PEO} and $R_{tot.}$ is represented by the shaded area.

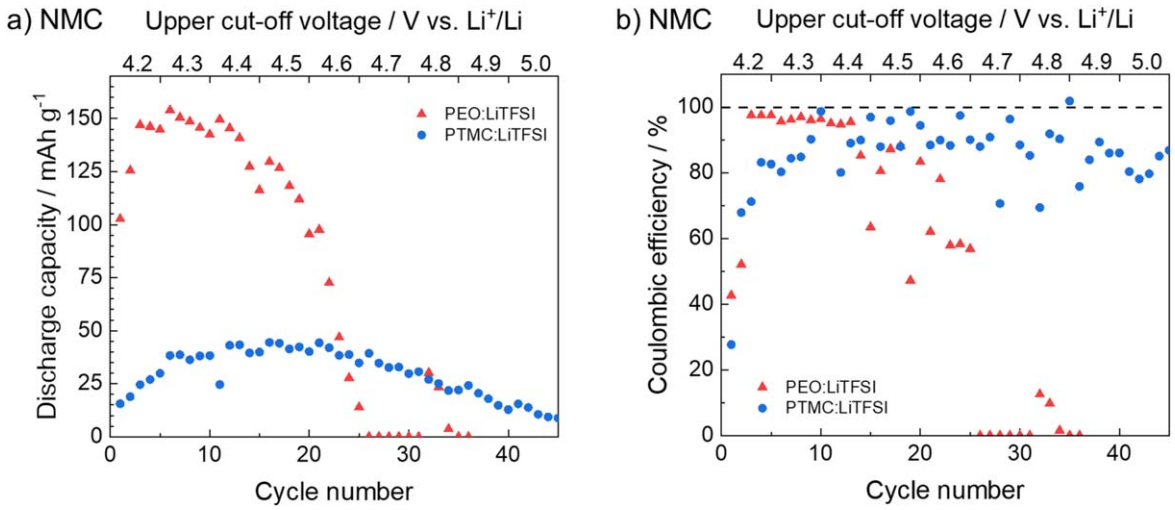

Figure 8. Results from CICC experiments for NMC half-cells: a) discharge capacity and b) Coulombic efficiency. The first employed upper cut-off voltage is 4.2 V vs Li^+/Li and it was thereafter increased by 0.1 V every 5 cycles until 5 V vs Li^+/Li or until battery failure.

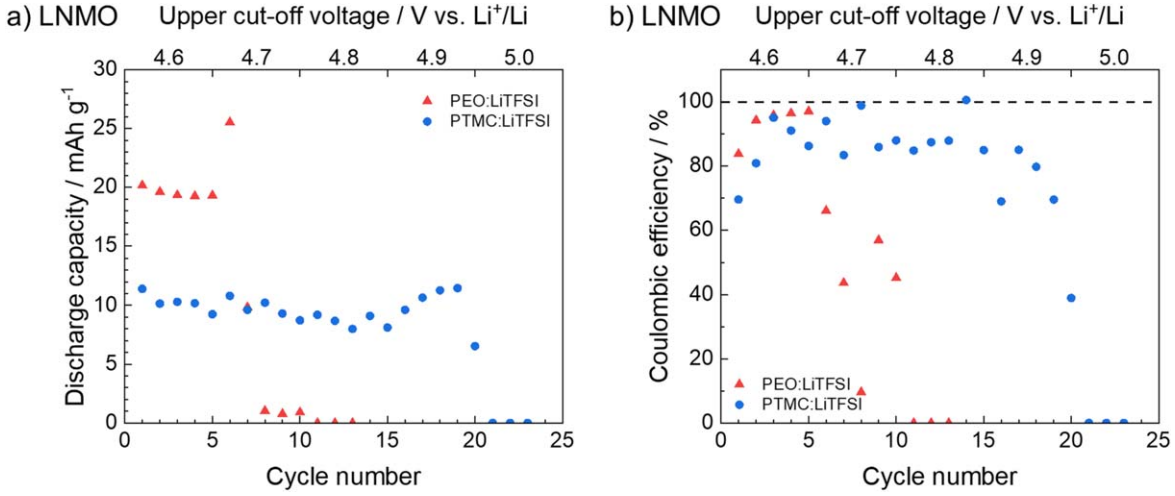

Figure 9. Results from CICC experiments for LNMO half-cells: a) discharge capacity and b) Coulombic efficiency. The first upper cut-off voltage employed is 4.6 V vs Li^+/Li and it was thereafter increased by 0.1 V every 5 cycles until 5 V vs Li^+/Li or until battery failure.

cases the failure characteristics are similar with an abrupt drop in voltage (Fig. S11).

Although the CICC method provides a wide overview of the performance of each polymer electrolyte with different active materials at different voltages, it is not without limitations. One of those is that the technique does not differentiate electrolyte degradation from battery ageing during cycling or degradation taking place at the lithium metal counter electrode. In addition, due to the different properties and consequently overpotential with each SPE, it could be argued that PEO:LiTFSI spends more time at certain voltage compared to PTMC:LiTFSI, which can also trigger more pronounced decomposition. Additionally, with CICC as well as with CV, SV or SCPV, it is difficult to say to what degree the current response for PTMC:LiTFSI and PEO:LiTFSI is influenced by the presence of impurities such as H_2O. During the first cycle of all CV measurements, a small current is generated which is not present in following cycles, see Fig. S3. This small peak is more pronounced for PEO:LiTFSI compared to PTMC:LiTFSI. In PTMC:LiTFSI, H_2 evolution synonymous with water oxidation has previously been observed at 4.4 V vs Li^+/Li against a carbon cloth working electrode.[31] Since the stainless steel working electrode used for the CV, SV and SCPV measurements has a higher electrocatalytic activity for H_2 evolution compared to carbon,[36] oxidation currents originating from water oxidation can be expected at slightly lower oxidation potentials, thereby overlapping with many of the oxidation onsets reported herein. However, the H_2O concentration has previously been estimated to 40 ppm in PTMC:LiTFSI (produced using the same synthesis method as in this work), and hence a limited effect can be expected.[37] In contrast, much higher concentrations have been reported in PEO:LiTFSI, thereby making it difficult to ascertain the true stability of this system.[38] Furthermore, it is not certain to what extent H_2O can trigger secondary side reactions and contribute to additional SPE decomposition at higher potentials. Notwithstanding, one could argue that the impurities are an integral part of the SPE system and should be treated as such when assessing the practical stability of the electrochemical system.

From the summary of all measurements with the different techniques in Table I, it is clear that LSV, SV and CICC measurements all lead to different values of the oxidative stability for PEO:LiTFSI and PTMC:LiTFSI and they are also different from the results from SCPV. While CV shows higher oxidative stability for PEO:LiTFSI than PTMC:LiTFSI, the opposite is observed with SV. SCPV shows that PEO:LiTFSI passes more charge, i.e. has a lower oxidative stability, than PTMC:LiTFSI when following the LFP and NMC voltage profiles but the opposite is observed for the

Table I. Experiment conditions for LSV, SV and CICC measurements and oxidative stability of PTMC:LiTFSI and PEO:LiTFSI at 60 °C according to LSV, SV and CICC. Since SCPV does not identify an onset potential, this technique has been omitted from the comparison.

Technique	Working electrode	Potential range V vs Li^+/Li	Scan rate	PTMC:LiTFSI V vs Li^+/Li	PEO:LiTFSI V vs Li^+/Li
CV	Stainless steel	3−5	10 mV s^{-1}	4.4	4.7
	”	”	1 mV s^{-1}	4.5	4.8
	”	”	0.1 mV s^{-1}	4.3	4.8
SV	”	”	100 mV step h^{-1}	3.8	3.5
CICC	LFP	2.7–3.7…5	C/20	3.8	4.3
	NMC	3.5–4.2…5	C/20	4.6	4.5
	LNMO	3.5–4.6…5	C/20	4.8	4.7

LNMO profile, indicating the effect of the voltage profile on the anodic stability. Regarding the CICC method, it is also clear that the active material influences the oxidative stability of the cell. For LFP electrodes, PEO:LiTFSI shows higher oxidative stability than PTMC:LiTFSI, while for NMC and LNMO PTMC:LiTFSI features superior oxidative stability to PEO:LiTFSI. These results with CICC indicate that the active material is a highly relevant factor to consider in electrochemical stability investigations. In addition, the surface chemistry and the interphase build-up during cycling will also contribute to the practical stability of the system.

Another general observation when comparing both SPEs is that for PEO:LiTFSI the oxidative stability range reported for CV and CICC is between 4.3 and 4.8 V vs. Li^+/Li (with 3.5 V vs Li^+/Li for SV), which is narrower than the values found in literature 3.8–5.7 V vs Li^+/Li,[23–27] and closer to the oxidative stability of 4.6 V vs Li^+/Li reported for PEO:LiTFSI in half-cells with different active materials.[5] In the case of PTMC:LiTFSI, the oxidative stability range obtained with each technique is broader from 3.8 to 4.8 V vs Li^+/Li and lower than the only value reported in literature of 5 V vs Li^+/Li.[18] These results clearly show how each technique as well as the cell setup influences the measured oxidative stability.

So, is it fair to refer to any of these values as *the* electrochemical stability limit of either SPE? We would argue that as any changes in the electrochemical setup will impact the determined stability limit —even when the measurements are meticulously performed—it is in fact not really relevant to refer to a stability limit of the electrolyte. Rather, it is much more appropriate to discuss the electrochemical stability limits of the *entire electrochemical system,* thus deliberately including also the catalytical effects of the working electrode and more closely approaching a relevant electrochemical setup from a battery operation point of view.

Conclusions

Through a comparison of cyclic voltammetry (CV), staircase voltammetry (SV), synthetic charge–discharge profile voltammetry (SCPV) and cut-off increase cell cycling (CICC), the electrochemical stability of PEO:LiTFSI and PTMC:LiTFSI as two representative SPEs has been determined. The results show that the anodic stability lies in a broad range depending on the technique and cell setup, with SCPV even indicating decomposition reactions on long timescales at even lower potentials. The side reactions and cell failures detected clearly show that the often reported results of SPE stabilities way above 5 V vs Li^+/Li likely say very little about the true electrochemical stability of these electrolytes. However, the failure of any single technique to determine an absolute electrochemical stability for these electrolytes becomes obvious when comparing these widely differing results obtained using the different techniques and measurement setups. While staircase voltammetry eliminates the mass transport limitations that exist for CV and LSV, and can approach a thermodynamic equilibrium at each potential, it is still not sufficient as the time spent at each voltage does not mimic the cycling conditions in a battery device. This is then considered with the SCPV technique; however, the working electrode is still not relevant for battery applications. Considering this, it becomes less meaningful to discuss the electrochemical stability of the electrolytes themselves. Instead, they need to be assessed in the electrochemical environment in which they are meant to be utilized. In this context it makes more sense to consider the electrochemical stability of the entire electrochemical system—i.e., the combination of electrode and electrolyte—as a whole. CICC targets such a more realistic system, but is of course itself not immune to all of the issues plaguing more conventional techniques, such as how to objectively determine when a signal is deviating from the baseline. There is also the added issue of inherent ageing of the cell when increasing the cycle number together with the cut-off voltage.

This goes to show that there is not a single and appropriate technique or method to definitely measure the ESW of SPEs. With this in mind, it becomes largely meaningless to discuss the electrochemical stability of SPEs isolated from the electrochemical system in which they are intended to be used. To treat the electrochemical stability on a system level, methods such as CICC represent an important step towards more reliable and relevant estimations of electrochemical stability for both solid- and liquid-state electrochemical systems.

Acknowledgments

This work has been financed through support from the ERC, grant no. 771777 FUN POLYSTORE. We also acknowledge support from STandUP for Energy and Batteries Sweden (Vinnova 2019–00064). Matthew J. Lacey is acknowledged for helpful discussions.

ORCID

Guiomar Hernández https://orcid.org/0000-0002-2004-5869
Alma Mathew https://orcid.org/0000-0002-0512-6820
Christofer Sångeland https://orcid.org/0000-0002-3374-2276
Daniel Brandell https://orcid.org/0000-0002-8019-2801
Jonas Mindemark https://orcid.org/0000-0002-9862-7375

References

1. J. R. Nair, L. Imholt, G. Brunklaus, and M. Winter, *Electrochem. Soc. Interface*, **28**, 55 (2019).
2. J. Kalhoff, G. G. Eshetu, D. Bresser, and S. Passerini, *Chem. Sus. Chem*, **8**, 2154 (2015).
3. L. Frenck, G. K. Sethi, J. A. Maslyn, and N. P. Balsara, *Front. Energy Res.*, **7**, 115 (2019).
4. G. Homann, L. Stolz, M. Winter, and J. Kasnatscheew, *iScience*, **23**, 101225 (2020).
5. G. Homann, L. Stolz, J. Nair, I. C. Laskovic, M. Winter, and J. Kasnatscheew, *Sci. Rep.*, **10**, 4390 (2020).
6. R. Khurana, J. L. Schaefer, L. A. Archer, and G. W. Coates, *J. Am. Chem. Soc.*, **136**, 7395 (2014).
7. P. Peljo and H. H. Girault, *Energy Environ. Sci.*, **11**, 2306 (2018).
8. K. Xu, *Chem. Rev.*, **114**, 11503 (2014).
9. C. F. N. Marchiori, R. P. Carvalho, M. Ebadi, D. Brandell, and C. M. Araujo, *Chem. Mater.*, **32**, 7237 (2020).
10. K. Xu, S. P. Ding, and T. R. Jow, *J. Electrochem. Soc.*, **146**, 4172 (1999).
11. A. Méry, S. Rousselot, D. Lepage, and M. Dollé, *Materials (Basel).*, **14**, 3840 (2021).
12. K. Xu, M. S. Ding, and T. Richard Jow, *Electrochim. Acta*, **46**, 1823 (2001).

13. M. P. S. Mousavi, A. J. Dittmer, B. E. Wilson, J. Hu, A. Stein, and P. Bühlmann, *J. Electrochem. Soc.*, **162**, A2250 (2015).
14. E. J. Olson and P. Bühlmann, *J. Electrochem. Soc.*, **160**, A320 (2013).
15. J. Kasnatscheew, B. Streipert, S. Röser, R. Wagner, I. Cekic Laskovic, and M. Winter, *Phys. Chem. Chem. Phys.*, **19**, 16078 (2017).
16. E. Fedeli, O. Garcia-Calvo, T. Thieu, T. N. T. Phan, D. Gigmes, I. Urdampilleta, and A. Kvasha, *Electrochim. Acta*, **353**, 136481 (2020).
17. L. Stolz, G. Homann, M. Winter, and J. Kasnatscheew, *Mater. Adv.*, **2**, 3251 (2021).
18. B. Sun, J. Mindemark, K. Edström, and D. Brandell, *Solid State Ionics*, **262**, 738 (2014).
19. J. Mindemark, E. Törmä, B. Sun, and D. Brandell, *Polymer*, **63**, 91 (2015).
20. M. J. Lacey, *ChemElectroChem*, **4**, 1997 (2017).
21. Y. C. Chien, A. S. Menon, W. R. Brant, D. Brandell, and M. J. Lacey, *J. Am. Chem. Soc.*, **142**, 1449 (2020).
22. M. P. Rosenwinkel, R. Andersson, J. Mindemark, and M. Schönhoff, *J. Phys. Chem. C*, **124**, 23588 (2020).
23. D. T. Hallinan and N. P. Balsara, *Annu. Rev. Mater. Res.*, **43**, 503 (2013).
24. H. Cheng, C. Zhu, B. Huang, M. Lu, and Y. Yang, *Electrochim. Acta*, **52**, 5789 (2007).
25. S. Sylla, J. Y. Sanchez, and M. Armand, *Electrochim. Acta*, **37**, 1699 (1992).
26. J.-H. Shin, W. A. Henderson, and S. Passerini, *J. Electrochem. Soc.*, **152**, A978 (2005).
27. Z. Li, Y. Zhao, and W. E. Tenhaeff, *ACS Appl. Energy Mater.*, **2**, 3264 (2019).
28. J. Qiu et al., *Adv. Funct. Mater.*, **30**, 1909392 (2020).
29. Z. Li, Y. Zhao, and W. E. Tenhaeff, *Chem. Mater.*, **33**, 1927 (2021).
30. B. Sun, J. Mindemark, K. Edström, and D. Brandell, *Electrochem. Commun.*, **52**, 71 (2015).
31. C. Sångeland, B. Sun, D. Brandell, E. J. Berg, and J. Mindemark, *Batter. Supercaps, Batt.*, **4**, 785 (2021).
32. M. He, L. Hu, Z. Xue, C. C. Su, P. Redfern, L. A. Curtiss, B. Polzin, A. von Cresce, K. Xu, and Z. Zhang, *J. Electrochem. Soc.*, **162**, A1725 (2015).
33. C. Z. Zhao, Q. Zhao, X. Liu, J. Zheng, S. Stalin, Q. Zhang, and L. A. Archer, *Adv. Mater.*, **32**, 1905629 (2020).
34. A. Mathew, M. J. Lacey, and D. Brandell, *J. Power Sources Adv.*, **11**, 100071 (2021).
35. R. Asakura, L. Duchêne, R. S. Kühnel, A. Remhof, H. Hagemann, and C. Battaglia, *ACS Appl. Energy Mater.*, **2**, 6924 (2019).
36. R. Koutavarapu, C. V. Reddy, B. Babu, K. R. Reddy, M. Cho, and J. Shim, *Int. J. Hydrogen Energy*, **45**, 7716 (2020).
37. B. Sun, C. Xu, J. Mindemark, T. Gustafsson, K. Edström, and D. Brandell, *J. Mater. Chem. A*, **3**, 13994 (2015).
38. C. Xu, B. Sun, D. Brandell, and M. Hahlin, *J. Mater. Chem. A*, **2**, 7256 (2014).